Available online at www.sciencedirect.com
SCIENCE DIRECT
Journal of Power Sources 146 (2005) 310–314
JOURNAL OF POWER SOURCES
www.elsevier.com/locate/jpowsour

Synthesis of metal-doped todorokite-type MnO_2 and its cathode characteristics for rechargeable lithium batteries

Naoaki Kumagai *, Shinichi Komaba, Kiyoko Abe, Hitoshi Yashiro

Graduate School of Engineering, Iwate University, Morioka 020-8551, Japan

Available online 31 May 2005

Abstract

Todorokite-type MnO_2-doped with Co and Fe has been synthesized by hydrothermal treatment of layered metal-doped manganese oxide, buserite, in water at 120–200 °C. The prepared todorokite products have been characterized by XRD and energy dispersive X-ray spectroscopic (EDX) measurements, TEM observation and thermogravimetric analysis. These measurements showed that the hydrothermal products are the metal-doped todorokite phase having large (3 × 3) tunnel structure, and the chemical compositions are shown to be $Mg_xM_yMn_{1-y}O_2{\cdot}zH_2O$, where $x = 0.08$–0.10, $y = 0.23$–0.29, $z = 0.35$–0.54 in M = Co and $x = 0.13$–0.14, $y = 0.03$–0.16, $z = 0.19$–0.28 in M = Fe. The preliminary electrochemical characteristics including charge–discharge cyclings of the metal-doped-todorokite electrodes were examined as lithium insertion hosts for cathodes in rechargeable lithium batteries. The metal-doped todorokite exhibited S-shaped discharge behavior and the Co-doped one with $x = 0.10$, $y = 0.29$ showed a high discharge capacity of ca. 132 mAh g^{-1}-oxide and cycling capacity of 90–100 mAh g^{-1}.

Keywords: Manganese oxide; Metal-doped todorokite; Lithium battery

1. Introduction

Manganese oxides have been studied for long time for use in battery application. There are various manganese-based oxide frameworks, which are roughly classified into one-dimensional tunnel structure, layered structure and three-dimensional spinel structure [1]. The todorokite-type MnO_2 has the largest tunnel structure, which consists of triple chains of edge-sharing MnO_6 octahedera that form 3×3 tunnel [1,2]. Previously, Chen et al. have synthesized a thermally stable todorokite-type MnO_2 by means of the combination of aqueous solution and hydrothermal techniques [3], and Zhou et al. have prepared the todorokite-doped by several transition metals into the framework for using as molecular sieve materials [4]. Furthermore, the electrochemical behavior of the todorokite-type MnO_2 has been studied for cathode materials in lithium batteries [5–7]. In our previous work, we reported the preparation of the todorokite-type MnO_2 and its application as a cathode for lithium and magnesium rechargeable batteries [8]. In this work, we report the preparation of the todorokite-type MnO_2-doped by Co and Fe ions in the framework and the cathode characteristics in rechargeable lithium batteries.

2. Experimental

The metal-doped todorokite manganese oxides were prepared according to the previous literature [8] as follows: at first, in order to synthesize metal-doped layered birnessite, $(Mn_{1-y}M_y)(OH)_2$, was precipitated by addition of 50 ml of 5.0 mol dm^{-3} NaOH solution into 40 ml of 0.50 mol dm^{-3} $MnCl_2 + MCl_2$ (M = Co, Fe) solution with several molar ratios of M/(Mn + M) under vigorus stirring at room temperature, as shown in Table 1. This $Mn_{1-y}M_y(OH)_2$ (M = Co or Fe) was oxidized by adding 0.1 mol dm^{-3} $NaMnO_4$ at molar ratio of $Mn_{1-y}M_y(OH)_2/NaMnO_4 = 0.4$ at room temperature to obtain metal-doped birnessite powder. The precipitates were filtered and dried at room temperature for 1 day. Ion-exchange of the Na^+ for Mg^{2+} in the interlayer space was achieved by dispersing the birnessite in 1.0 mol dm^{-3} $MgCl_2$

* Corresponding author. Tel.: +81 19 621 6328; fax: +81 19 621 6328.
E-mail address: nkumagai@iwate-u.ac.jp (N. Kumagai).

0378-7753/$ – see front matter © 2005 Elsevier B.V. All rights reserved.
doi:10.1016/j.jpowsour.2005.03.145

Table 1
Reaction conditions for preparing the birnessite products, and hydrothermal temperature and chemical compositions of the todorokite products

Sample no.	Reaction condition[a]			Todorokite product[b]	
	Aqueous solution	(M/(Mn + M)) × 100 (%)	Temperature (°C)	Hydro-thermal temperature (°C)	Chemical composition
1	$MnCl_2$	0	r.t.[c]	160	$Mg_{0.11}MnO_2{\cdot}0.32H_2O$
2	$MnCl_2 + CoCl_2$	5	r.t.	160	$Mg_{0.08}Co_{0.23}Mn_{0.77}O_2{\cdot}0.37H_2O$
3	$MnCl_2 + CoCl_2$	10	r.t.	160	$Mg_{0.10}Co_{0.29}Mn_{0.71}O_2{\cdot}0.35H_2O$
4	$MnCl_2 + CoCl_2$	20	r.t.	160	$Mg_{0.08}Co_{0.26}Mn_{0.74}O_2{\cdot}0.54H_2O$
5	$MnCl_2 + FeCl_2$	5	r.t.	160	$Mg_{0.14}Fe_{0.03}Mn_{0.97}O_2{\cdot}0.28H_2O$
6	$MnCl_2 + FeCl_2$	10	r.t.	160	$Mg_{0.13}Fe_{0.16}Mn_{0.84}O_2{\cdot}0.19H_2O$

[a] The birnessite products were dried at about 23 °C for 24 h.
[b] The todorokite products were dried at 80 °C for 24 h.
[c] r.t.: room temperature (about 23 °C).

solution for 1 day at 25 °C to obtain the metal-doped buserite. Todorokite $Mg_xMn_{1-y}M_yO_2{\cdot}zH_2O$ was prepared by hydrothermal treatment (120–200 °C) of the Mg buserite for 4 days in pure water. Finally, the products were dried at 80 °C.

The obtained samples were identified by powder X-ray diffraction (XRD) using a Rigaku Rint 2200 diffractometer with Cu Kα radiation. Energy dispersive X-ray spectroscopic (EDX; 20 kV, Hitachi, S-2300) measurements were performed to observe the morphology of particles and analyse the composition of particles. Transmission electron microscopic (TEM; 200 kV, Hitachi, H-800) measurements were carried out to observe the morphology of samples. Thermogravimetric (TG) measurements were carried out using Seiko Electronic Industry TG/DTA 320 at heating rate of 10 °C min^{-1} in air. The elemental analyses of obtained samples were carried out by atomic absorption spectroscopy to determine Mg, Mn, Co and Fe contents. The water content was measured from weight loss by heating at 300 °C for 1 h.

Electrochemical lithium insertion/deinsertion was investigated using coin-type cell. For electrode preparation, the prepared powders were mixed with 5 wt.% of graphite, 10 wt.% of acetylene black and 5 wt.% of polyvinylidine fluoride binder in *N*-methyl pyrolidinone. This mixture was pasted onto a aluminum foil (1.0 cm × 1.0 cm) and then vaccum dried at 80 °C for 1 day. Lithium foils were used as counter electrodes. The electrolyte used was 1 mol dm^{-3} $LiPF_6$/EC + DEC (1:1). The discharge and charge–discharge cyclings were carried out between 2.0 and 4.2 V at 0.1 mA cm^{-2} and 25 ± 1 °C.

3. Results and discussion

The reaction conditions for preparing the birnessite products are given in Table 1. In any aqueous solution consisting of $MnCl_2$ or $MnCl_2 + MCl_2$ (M = Co or Fe) in several M/(Mn + M) ratios, the birnessite-type MnO_2 and its metal-doped birnessite phases were confirmed by XRD measurement. Then, the several birnessite products were ion-exchanged in 1.0 mol dm^{-3} $MgCl_2$ solutions for 1 day, and the products were dried in the temperature range from 0 to 80 °C in air for 1 day. The Na^+ ions of the undoped birnessite dried at 0–80 °C were easily ion-exchanged with Mg^{2+} ions to form the Mg-buserite phase. In the case of Co-doped birnessite products, however, the ion exchanging of the Na^+ ions for Mg^{2+} ions occurred only for the Co-doped birnessite dried at a lower temperature below room temperature, leading to the Co-doped buserite phase, which was confirmed by the XRD measurement. Thus, for preparing the metal-doped Mg^{2+}-buserite precursors, the metal-doped birnessite products were dried at room temperature for 1 day.

The hydrothermal treatment of the buserite and its Co- and Fe-doped products were carried out for 4 days in pure water in the temperature range from 120 to 200 °C. The XRD patterns of products obtained by treatment at 160 °C are shown in Fig. 1, and their chemical compositions are given in Table 1. In the XRD pattern (a) of non-metal-doped sample (no. 1 in Table 1), the peaks corresponding to the todorokite MnO_2 phase appear at 2θ = about 9°, 19°, 26° and 37° [6,8]. These four peaks are indexed as (0 0 1), (0 0 2), (0 0 3) and (0 0 4) diffraction, respectively, by assuming todorokite samples have a pseudo-orthorhombic cell [3]. For the Co-doped sample (no. 2–4) and Fe-doped samples (no. 5 and 6), the XRD patterns (b–f) quite similar to the undoped one (a) are observed, indicating that metal-doped todorokite phases are produced through hydrothermal treatment of the metal-doped buserite. However, as seen in Fig. 1, the 0 0 3 peak almost disappears at higher metal dopant amount (c, d and f), although it is clearly observed in the case of Co-doped no. 3 sample (b). Moreover, the shape of the 0 0 3 peak at lower metal dopant amount (b and e) is distinctly sharp compared to non-doped (a) and different from those of the other 0 0 l peaks.

As reported in the previous papers [6–8], the appearance of the 0 0 3 peak of todorokite phase depended on the preparation condition and the kind of cation in the (3 × 3) tunnel. In the todorokite obtained from birnessite precursor prepared using O_2 oxidation, the 0 0 3 peak was not observed [7]. We reported that todoroke phase prepared from hydrothermal treatment of Mg-busserite at a lower temperature of 120 °C did not show the 0 0 3 peak [8]. Moreover, Yang et al. [6] showed that Mg-todorokite shows distict 0 0 3 peak, but Co-todorokite does not show it at all. Thus, metal doping

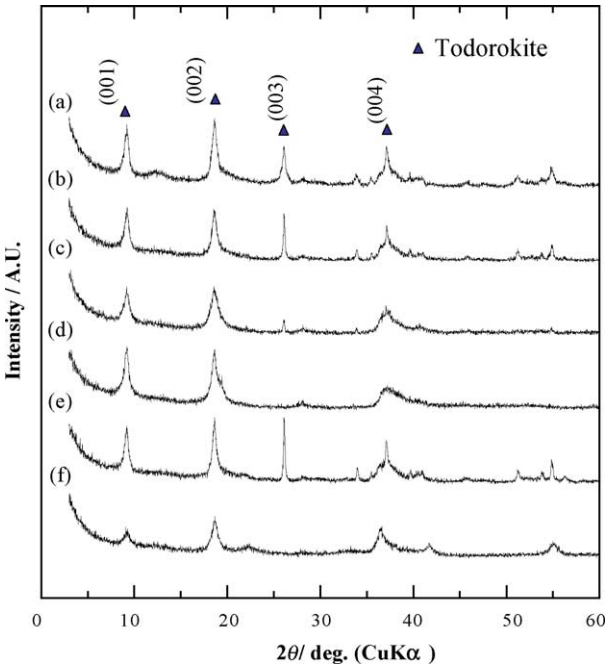

Fig. 1. X-ray diffraction patterns of the todorokite samples formed from hydrothermal treatment of the buserite products at 160 °C: (a) non-metal-doped sample (no. 1 in Table 1), (b) Co-doped sample (no. 2), (c) Co-doped sample (no. 3), (d) Co-doped sample (no. 4), (e) Fe-doped sample (no. 5) and (f) Fe-doped sample (no. 6).

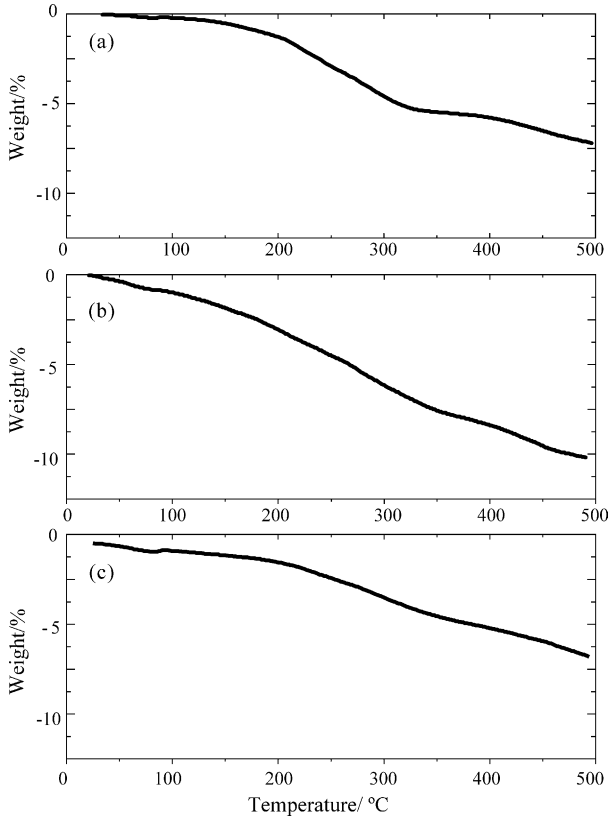

Fig. 3. TG curves of the todorokite samples for (a) non-metal-doped sample (no. 1 in Table 1), (b) Co-doped sample (no. 3) and (c) Fe-doped sample (no. 6).

to the todorokite structure would cause the variation in the intensity and shape of the 0 0 3 peak. That is, it is seemed that a part of doping metals may be incorporated into the (3 × 3) tunnel structure, resulting in the variation of the 0 0 3 peak. Furthermore, the XRD patterns of products obtained from hydrothermal treatment of Co- and Fe-doped buserites at 120 and 200 °C were considerably similar to those of the hydrothermal products at 160 °C (Fig. 1).

The chemical compositions of the todorokite products formed from hydrothermal treatment of the buserite products at 160 °C are given in Table 1. In the metal-doped products (no. 2–6), the compositions are shown to be $Mg_xM_yMn_{1-y}O_2{\cdot}zH_2O$, where $x = 0.08$–0.10, $y = 0.23$–0.29, $z = 0.35$–0.54 in M = Co (no. 2–4) and $x = 0.13$–0.14, $y = 0.03$–0.16, $z = 0.19$–0.28 in M = Fe (no. 5 and 6). The amounts of Mg^{2+} ions in the Co- and Fe-doped products are close to that in the undoped one, and the Mg^{2+} ions hydrated by water molecules would be incorporated in the large [3 × 3] tunnels [1,2]. It is found that the Co content in the products (no. 2–4) are considerably higher than the Fe content in the products (no. 5 and 6) obtained in the same preparation condition, and the Co and Fe ions are probably incorporated mainly into the todorokite framework by substituting Mn ions.

The TEM images of the todorokite and its metal-doped samples are given in Fig. 2. It is observed that the undoped todorokite mainly consists of needle-like crystals with the thickness of 20–40 nm (a). On the other hand, the Co- and

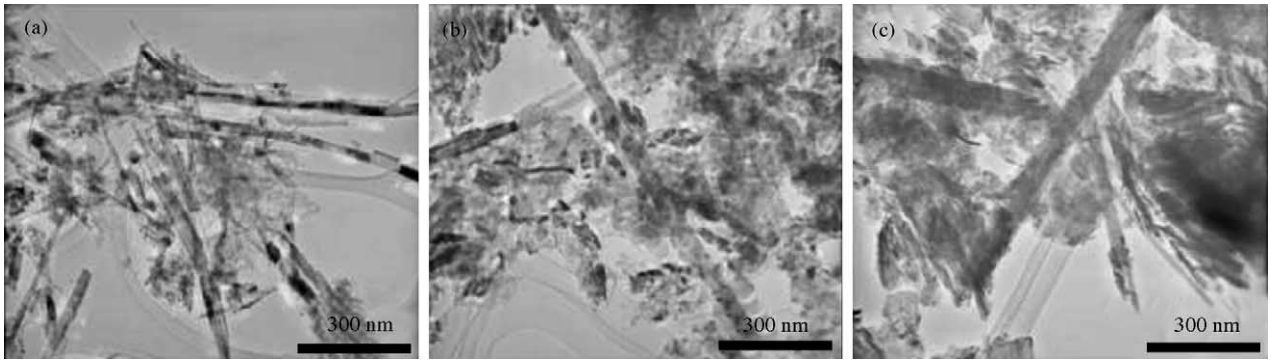

Fig. 2. TEM images of the todorokite samples for (a) non-metal-doped sample (no. 1 in Table 1), (b) Co-doped sample (no. 3) and (c) Fe-doped sample (no. 5).

Fe-doped samples (b and c) consist of different particle forms of fine powders and needle-like crystals. The amount of fine powder particles in Co- and Fe-doped samples (b and c) is significantly larger than that of the undoped one (a). This suggests that the existence of Co and Fe ions in the buserite product restrains the crystallization of the todorokite phases during hydrothermal reaction in water, resulting in fine powder product. To examine the Mg, Mn and M (M = Co, Fe) ingredients in the prepared powder, scanning TEM (STEM) element analysis was carried out to obtain corresponding energy-dispersive spectroscopic (EDS) elemental maps of Mg, Mn and Co for the $Mg_{0.10}Co_{0.29}Mn_{0.71}O_2{\cdot}0.35H_2O$ and Mg, Mn and Fe for the $Mg_{0.14}Fe_{0.03}Mn_{0.97}O_2{\cdot}0.28H_2O$. It was clearly observed from the pictures in 100 μm scale that the M (M = Co, Fe), Mn and Mg ingredients were uniformly distributed throughout the oxide particles. This confirms the existence of Co and Fe components.

The TG curves of the todorokite and its metal-doped samples are shown in Fig. 3. In these samples, the weight decrease of about 4–7% occurs on heating up to around 350 °C, followed by a gradual decrease of 1.5–2.5% up to 500 °C. The non- and metal-doped todorokite samples, heat-treated at 200, 300 and 500 °C for 1 h in air, were examined by XRD measurements. The XRD measurements of the heat-treated samples indicated that the original structures of non- and metal-doped todorokite samples are almost maintained on heating up to 300 °C. Furthermore, on heating up to 500 °C, the non- and metal-doped todorokite samples are decomposed mainly into $MgO{\cdot}Mn_2O_3$ and Mn_2O_3. Thus, the large weight loss of 4–7% up to around 300 °C is mainly due to the loss of adsorbed water and hydrated water in the large tunnels of the non- and metal-doped todorokites. The gradual weight loss of about 2% at 350–500 °C is probably due to the dehydroxylation of layer OH and to the departure of water, and to the reduction of manganese leading to the formation of Mn_2O_3 and its related compounds.

These undoped and metal-doped todorokite samples were examined as lithium insertion hosts for cathode materials in lithium batteries. The initial discharge and charge–discharge cyclings of the todorokite samples were carried out at a current density of 10 mA g^{-1} and 25 °C, as shown in Fig. 4. As seen in the figure, the metal-doped samples (c, e, g and h) exhibit S-shaped discharge curves quite similar to the undoped one (a). The Co-doped (c and e) and Fe-doped (g and h) samples show initial discharge capacities of ca. 75 mAh g^{-1}-oxide corresponding to 0.28Li/(Mn + Co) and 73–90 mAh g^{-1} (0.26–0.31Li/(Mn + Fe)), respectively. It is found that the metal doping to the todorokite oxide generally causes the decrease in the discharge capacity. As discussed from the XRD measurements, a part of doping metal may

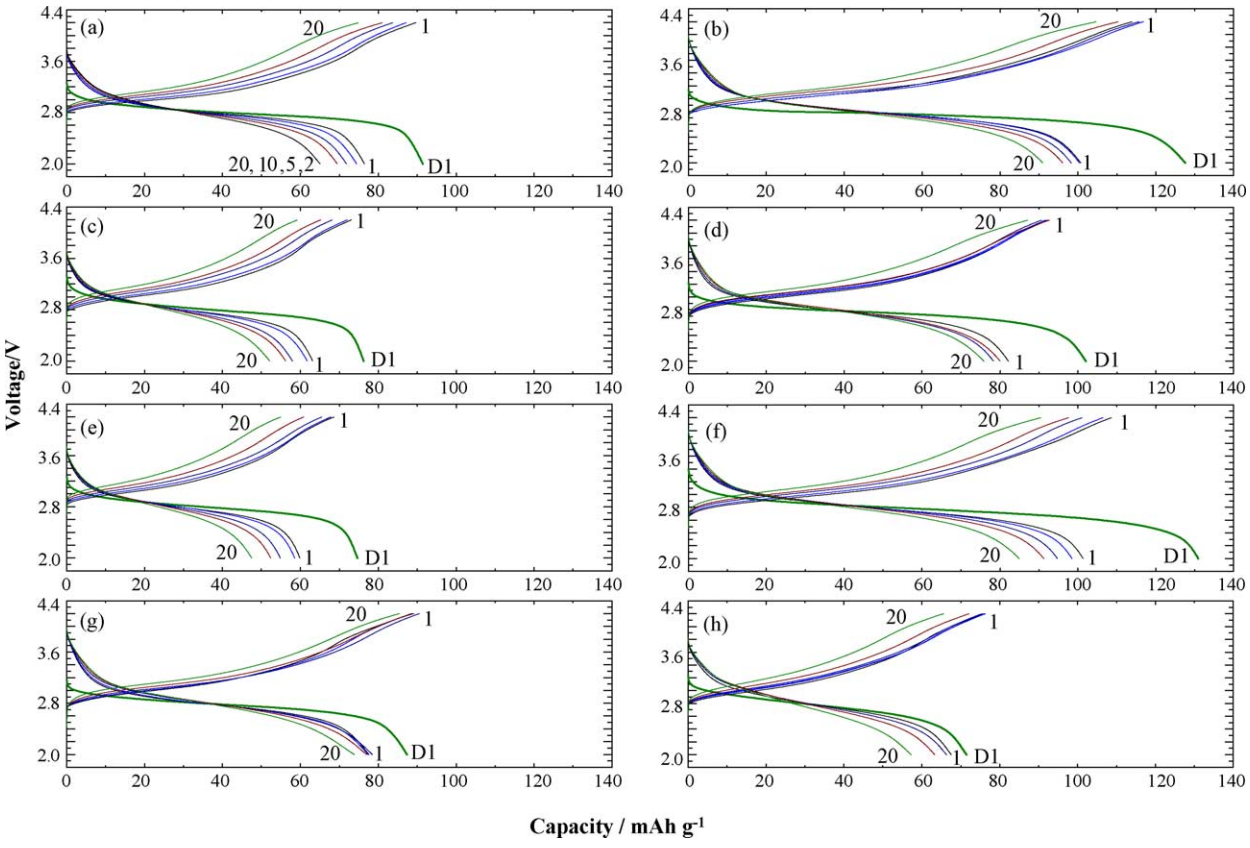

Fig. 4. Initial discharge and charge–discharge curves of the todorokite samples at a current density of 20 mA g^{-1} and 25 °C between 2.0 and 4.2 V: (a) non-metal-doped sample (no. 1 in Table 1), (b) sample no. 1 heat-treated at 200 °C for 1 h, (c) Co-doped sample (no. 2), (d) sample no. 2 heat-treated at 200 °C for 1 h, (e) Co-doped sample (no. 3), (f) sample no. 3 heat-treated at 200 °C for 1 h, (g) Fe-doped sample (no. 5) and (h) Fe-doped sample (no. 6).

be incorporated into the large (3×3) tunnel in the todorokite structure. This would hinder the lithium insertion into the structure, leading to decrease of the discharge capacity, especially at higher metal dopant amount (c, e and h). These discharge capacities of non- and metal-doped samples decreased gradually with cycling number. This would be due to the degradation of the crystal lattice arrangement of todorokite during lithium insertion/deinsertion [5]. The todorokite contains hydrated water molecules of Mg^{2+} ions in the tunnel structure [2]. As previously reported in our paper [8], the lithium insertion characteristics of the undoped todorokite were improved by removing the water because of the formation of the large vacant tunnel. Thus, the discharge and charge–discharge cyclings of the undoped and Co-doped todorokite samples, heat-treated at 200 °C for 1 h in air, were examined. As seen in Fig. 4, for the undoped and Co-doped samples (b, d, f), the discharge and cycling capacities are increased by the heat-treatment, and the Co-doped no. 3 sample heat-treated at 200 °C (f) showed high discharge capacity of ca. 132 mAh g^{-1} corresponding to ca. 0.47Li/(Mn + Co), and cycling capacity of ca. 85–100 mAh g^{-1} during 20 cyclings, corresponding to those of undoped sample (a). This may be due to the enhancement in the lithium diffusion kinetics in the tunnel structure.

Acknowledgments

The authors would like to thank Mrs. Nobuko Kumagai and Mr. S. Takahashi for the helpful assistance in the experimental work. This study was partially supported by Industrial Technology Research Grant Program from NEDE and Grant-in-Aid for Scientific Research (B) from JSPS in Japan.

References

[1] Q. Feng, H. Kanoh, K. Ooi, J. Mater. Chem. 9 (1999) 319.
[2] J.E. Post, D.L. Bish, Am. Mineral. 73 (1988) 861.
[3] Y.F. Chen, R.P. Zerger, R.N. DeGuzman, S.L. Suib, L. McCurdy, D.I. Potter, C.L. O'Young, Science 260 (1993) 511.
[4] H. Zhou, J.W. Wang, X. Chen, C.L.O. Young, S.L. Suib, Microporous Mesoporous Mater. 21 (1998) 315.
[5] Y. Yang, D. Shu, H. Yu, X. Xia, Z.G. Lin, J. Power Sources 65 (1997) 227.
[6] Y. Yang, D. Shu, H. Yu, J.K. Yon, Z.G. Lin, J. Power Sources 81/82 (1999) 637.
[7] M.J. Duncan, F. Leroux, J.M. Corbett, L.F. Nazar, J. Electrochem. Soc. 145 (1998) 3746.
[8] N. Kumagai, S. Komaba, H. Sakai, N. Kumagai, J. Power Sources 97/98 (2001) 515.